

# Domain formation and self-sustained oscillations in quantum cascade lasers

Tim Almqvist<sup>1</sup>, David O. Winge<sup>2</sup>, Emmanuel Dupont<sup>3</sup>, and Andreas Wacker<sup>1</sup>

<sup>1</sup> Mathematical Physics and NanoLund, Lund University, 22100 Lund, Sweden

<sup>2</sup> Synchrotron Radiation Physics and NanoLund, Lund University, 22100 Lund, Sweden

<sup>3</sup> Advanced Electronics and Photonics Research Centre, National Research Council, Ottawa, Ontario K1A 0R6, Canada

Received: July 22, 2022/ Revised version: NOT YET

**Abstract.** We study oscillations in quantum cascade lasers due to traveling electric field domains, which are observed both in simulations and experiments. These oscillations occur in a range of negative differential resistance and we clarify the condition determining whether the boundary between domains of different electric field can become stationary.

**PACS.** 05.45.-a Nonlinear dynamics and chaos – 42.55.Px Semiconductor lasers; laser diodes

## 1 Introduction

Quantum Cascade Lasers (QCLs)[1,2] have become the most important devices for radiation in the infrared region of the optical spectrum [3] and are also promising for THz applications [4]. They are based on electronic transitions between quantized states in the conduction band of semiconductor heterostructures, which enables a large flexibility to define the transition energy. QCLs are pumped electrically, where a sequence of scattering and tunneling transition fills the upper laser state and empties the lower one. While such an active module has a typical size of 50 nm, the repetition of a large number of modules (the name-giving cascade) allows to fill the optical waveguide with active material. Here the design is based on the assumption, that the applied bias drops homogeneously over all modules. However, tunneling between quantized states is prone to specific resonances [5] and the appearance of negative differential conductivity (NDC) for fields above the resonance point. In contrast to the resonant-tunneling diode [6], where this property is directly reproduced in the current-bias relation, the cascaded structure of QCLs provides an instability in the homogeneous voltage drop. This situation is analogous to the well-studied domain formation in Gunn diodes [7,8,9] and superlattices [10,11,12].

The formation of *stationary electrical field domains* in QCLs has been observed experimentally by the characteristic saw-tooth structure of the current-bias characteristics [13,14] and a spatially resolved measurement of the bias drop over the sample [15]. Oscillatory behavior has also been reported in the NDC region [16] which was, however, interpreted to be determined by the circuit similar to resonant tunneling diodes. Specifically, we consider the THz-QCL with scattering injection discussed in [17]. This structure exhibits characteristic regions of NDC in

the simulated current density  $J_{\text{hom}}(Fd)$  for identical bias drop  $Fd$  over all modules (so that periodic boundary conditions apply), as shown in Fig. 1. Experimentally, current plateaus are observed. Here we show, both by experiments and simulations, that *oscillating electric field domains* occur in our device, and discuss the conditions for their occurrence.

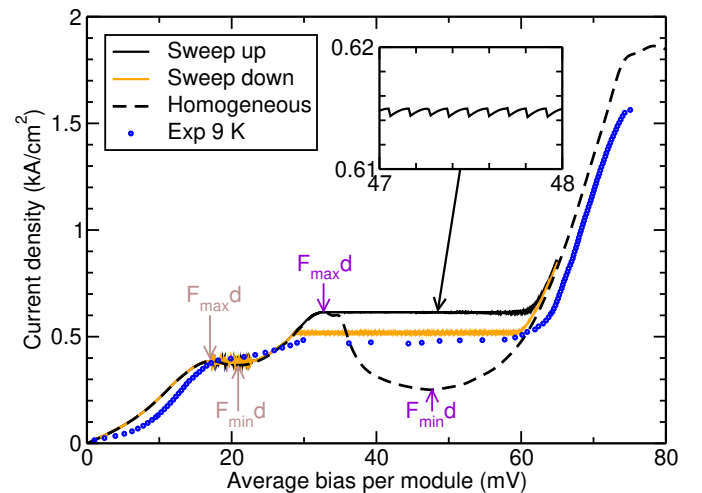


**Fig. 1.** Simulated current-bias relation with domain formation for a phonon temperature of 77 K.  $J_{\text{hom}}(Fd)$  (dashed line) is calculated by our NEGF simulation and shows two NDC regions between fields  $F_{\text{max}}$  and  $F_{\text{min}}$ , which denote maxima and minima of current. The full black/orange line shows the result with domain formation upon sweep-up/down of the bias, respectively. An enlarged section for sweep up is shown in the inset. The blue dots show corresponding experimental data.

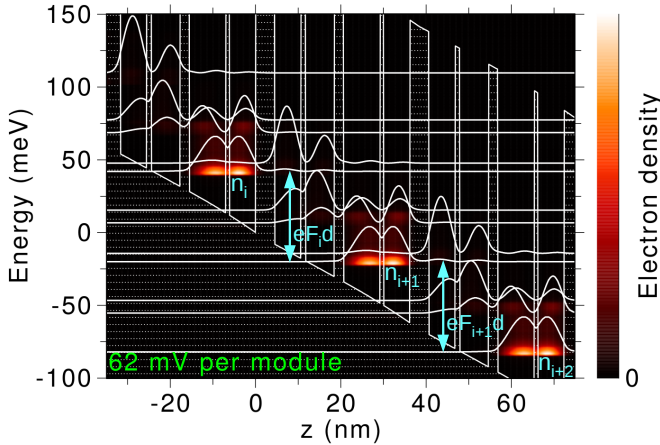


**Fig. 2.** Simulated electron density based on a homogeneous bias drop and description of the notation for electron sheet densities  $n_i$  and potential drop  $F_i d$ .

## 2 Simulating domain formation

In order to simulate domain formation, we assume that the sheet electron density  $n_i$  of each module is essentially confined in a narrow region before the thickest barrier. This is confirmed by our nonequilibrium Green’s function (NEGF) simulations as shown in Fig. 2. For details, see [18], where all parameters are given. As the only difference, we use an increased roughness height  $\eta = 3 \text{ \AA}$  here. The same location of charges was actually deduced experimentally [15]. The current to the next module is then essentially determined by the bias drop  $F_i d$ , where  $F_i$  is the average electric field between the electron densities located in module  $i$  and  $i + 1$  and  $d = 36.12 \text{ nm}$  is the thickness of a single module. Following a common approach in superlattices [11], this current density is approximated by

$$J_{i \rightarrow i+1} = J_{\text{hom}}(F_i d) \frac{n_i - n_{i+1} e^{-eF_i d/k_B T}}{N_d - N_d e^{-eF_i d/k_B T}}, \quad (1)$$

which assumes that the current density is essentially proportional to the electron density  $n_i$  in the injecting module and is reduced by a backward current from thermal excitations in the receiving module  $i + 1$ . This expression is normalized by the sheet doping density  $N_d = 3.25 \times 10^{10} \text{ cm}^{-2}$  per module, so that the homogeneous current is recovered for  $n_i = n_{i+1} = N_d$ . Then the continuity equation provides

$$e \frac{\dot{n}_i}{t} = J_{i-1 \rightarrow i} - J_{i \rightarrow i+1} \quad \text{for } i = 1, \dots, N \quad (2)$$

where  $N = 276$  is the number of modules.  $e$  is the positive elementary charge and we redefine the sign of electric field and current density, so that their signs match the forces and velocity of carriers, respectively. In Eq. (2) we need the boundary currents, which we approximate as

$$J_{0 \rightarrow 1} = \sigma F_0 \quad J_{N \rightarrow N+1} = \sigma F_N \frac{n_N}{N_d} \quad (3)$$

with a phenomenological boundary conductivity  $\sigma$ . Unless mentioned otherwise, we use  $\sigma/d = 50 \text{ A}/(\text{cm}^2 \text{ mV})$ , which is steeper than the slopes in  $j_{\text{hom}}(F d)$ . This mimics a good electrical contact with a small bias drop  $F_0 d$ . For given electron densities  $n_i$ , the electric fields are obtained from the total bias  $U$  dropping over the QCL

$$U = \sum_{i=0}^N F_i d \quad (4)$$

and Poisson’s equation

$$F_i - F_{i-1} = \frac{e}{\epsilon_0 \epsilon_r} (n_i - N_d) \quad \text{for } i = 1, \dots, N. \quad (5)$$

where  $\epsilon_r = 13$  is the average relative dielectric constant. For fixed bias  $U$ , this model has been applied for QCLs in [14]. Here we consider also the operation by a fixed bias source  $U_0$  via a serial load resistance  $R$ . Following [19] we find

$$\frac{U}{t} = \frac{1}{C_{\text{QCL}} + C_p} \left( \frac{U_0 - U}{R} - I \right) \quad (6)$$

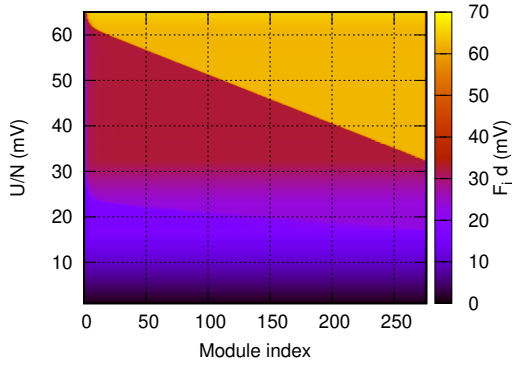
with  $I = \frac{A}{N + 1} \sum_{i=0}^N J_{i \rightarrow i+1}$

Here  $C_{\text{QCL}} = \epsilon_r \epsilon_0 A / (N + 1) d$  is the geometrical capacitance of the QCL structure with  $A = 0.144 \text{ mm}^2$  and  $C_p$  is an additional parallel capacitance, which we actually set to zero here.

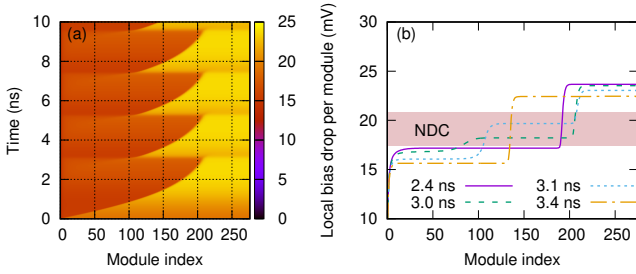
## 3 Simulation results

Figure 1 shows the simulated current bias relations using a fixed bias  $U$ . Upon sweeping up the bias, we find two current plateaus; after the first current peak around an average bias of 17 mV per module and also after the second current peak around an average bias of 33 mV per module. The current depends on the sweep direction, a common feature, which has been discussed for superlattices in detail, where multi-stability was observed [20]. The corresponding distribution of the electric field is shown in Fig. 3. Within the plateau regions, there are two domains with specific electric fields. An increase of bias is reflected in a shift of the domain boundary, where the high-field domain expands.

For the first plateau, the simulations provide actually oscillatory behavior as shown in Fig. 4. These are due to moving domain boundaries (also referred to as fronts), where the excess charge travels along the direction of electron motion. For  $J = 300 \text{ A}/\text{cm}^2$  we obtain an average drift velocity of  $J / (N_d e) = 60 \text{ modules}/\text{ns}$ , which is comparable to the average front velocity of 50 modules/ns observed in Fig. 4(a). During the motion of the domain boundary, the electric fields in both domains need to increase in order to maintain the fixed bias. Thus, the electric field in the low-field domain reaches eventually the NDC region (e.g.



**Fig. 3.** Simulated field distribution (in color scale) as a function of position and total bias, obtained by sweeping up the bias. (For  $U/N \sim 20$  mV the domain boundary oscillates in time and typical snapshots are displayed.)



**Fig. 4.** (a) Simulated field distribution (in color scale) as a function of position and time for a fixed average bias  $U/N = 19$  mV. Panel (b) shows the field distribution at particular times.

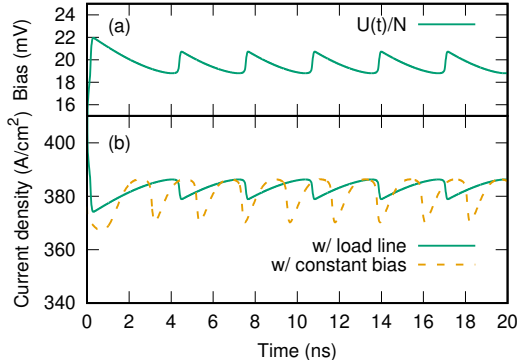


**Fig. 5.** (a) bias and (b) current density for simulations with  $R = 50 \Omega$  and  $U_0 = 33$  V in comparison with the bias controlled case (dashed) with  $U/N = 19$  mV as considered in Fig. 4.

at  $t \approx 3$  ns) and becomes unstable. Thus, a new accumulation layer is formed within a fraction of a nanosecond, which then starts its motion like the one before. If the sample is operated via a load resistor, the bias  $U$  is actually oscillating as shown in Fig. 5. In this case the oscillation frequency is reduced.

Such oscillations are generic for extended systems with NDC and have been well-studied for the Gunn Diode and

superlattices [9,21]. In continuous systems, such as the Gunn diode, any charge travels due to the drift velocity (albeit the actual speed may differ [8]) and thus no stationary fronts are possible. However, for discrete systems, such as superlattices and QCLs, these front can become stationary, so that the oscillations disappear [10,20,13]. Fig. 6 shows the electron density distribution close to the domain boundary in both plateaus. For the first plateau, see Fig. 6(b), the excess electron density  $n_{\text{excess}} = \epsilon_0 \epsilon_r (F_{\text{high}} - F_{\text{low}})/e$ , required to change the field between both domains, is spread out over several modules, which resembles the continuous case of the Gunn diode. In contrast, for the second plateau, see Fig. 6(a), a large part of the excess density is essentially located in one module and is trapped by the heterostructure, so that a stationary front appears [22]. This situation should be stable, if the NDC region is crossed within one module. Then at least the part  $n_{\text{NDC}} = \epsilon_0 \epsilon_r (F_{\text{min}} - F_{\text{max}})/e$  of  $n_{\text{excess}}$  is located within one module, where  $F_{\text{max/min}}$  denote the position of the current maximum/minimum at the borders of the NDC region, respectively, as indicated in Fig. 1. In order for this to happen, the current in a module with the excess density must match the current  $j$  of the other modules. Using the approximation for the current (1) under neglect of the backward current, this implies the condition for stationary accumulation fronts

$$\left( \frac{n_{\text{NDC}}}{N_d} + 1 \right) j_{\text{min}} \lesssim j, \quad (7)$$

where  $j_{\text{min}}$  is the minimum current in the NDC region. As the low-field domain is only possible for  $j < j_{\text{max}}$ , where  $j_{\text{max}}$  is the peak current before the NDC region we find the criterion for stationary domains with accumulation regions

$$\left( \frac{n_{\text{NDC}}}{N_d} + 1 \right) \lesssim \frac{j_{\text{max}}}{j_{\text{min}}}. \quad (8)$$

A thorough proof for the stability of stationary domains under this criterion is provided in [22]. Based on the homogeneous current-field relations in Fig. 1, we find  $n_{\text{NDC}}/N_d + 1 = 1.25$  for the first NDC region, which surpasses the ratio between peak and valley current  $j_{\text{max}}/j_{\text{min}} \approx 1.05$ . This agrees with finding only traveling fronts and oscillatory behavior in this plateau region. For the second plateau  $n_{\text{NDC}}/N_d + 1 = 1.92$  is lower than  $j_{\text{max}}/j_{\text{min}} \approx 2.44$  and stationary fronts are possible for currents above  $j = 1.92 j_{\text{min}} \approx 490$  A/cm<sup>2</sup> according to Eq. (7). This value agrees well with the minimal current density  $j_{\text{min}}^{\text{stat}} = 515$  A/cm<sup>2</sup> for the domain states upon sweeping down the bias in Fig. 1. In order to compare with experiment, it is important to realize that Eq. (1) is an approximation and that the minimum current density  $j_{\text{min}}$  is difficult to access. Furthermore, growth imperfections can shift the range of doping where oscillating field domains are observed in simulations for superlattices [23]. However, the condition (8) should reflect the most important trend, that stationary field domains require large doping densities and a pronounced peak to valley ratio.

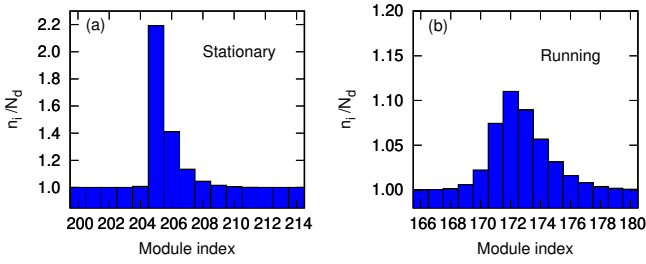


**Fig. 6.** Charge distribution of accumulation layer for domains at an average bias  $U/N = 40$  mV (left with stationary domain) and 19 mV (right with running domain)

### 4 Experimental results

The experimental data displayed in Fig. 1 show a clear current plateau in the second simulated NDC region (between 34 and 60 mV), while the current is monotonously increasing in the first simulated NDC region around 20 mV. Using a significantly different setup, Ref. [15] reported the occurrence of electric field domains in the second region but a homogeneous bias drop in the first region. This indicates, that the first (weak) NDC region seen in our simulations is not visible in the device. (It also vanishes in the simulations for an increased roughness  $\eta = 4$  Å or an elevated temperature of 150 K.) On the other hand, NDC and the formation of electric field domains is manifest in the pronounced second simulated NDC region.

Our measurements are based on 2  $\mu$ s long pulses and the device is operated via a load resistance of 40.7  $\Omega$  and the setup is described in [24]. However, a Si carrier with better quality is used here to solder the laser bar and its electrodes should not be resistive. Using a 1 GHz bandwidth oscilloscope, we observe oscillatory behavior in the bias as shown in Figs. 7(a,c). For a heatsink temperature of 80 K, regular oscillations are observed for external bias  $41.4 \text{ V} < U_0 < 48.5 \text{ V}$ . From 48.5 V to 49.5 V few sporadic, i.e. irregular, oscillations are observed. Above 49.5 V, few sporadic short surges of voltage are still observed indicating some voltage instabilities at the exit of the plateau. At the very beginning of the plateau, from 41.4 to 42.1 V, high amplitude oscillations at fundamental frequency  $\sim 27.6$  MHz are observed. At 42.1 V, as intense but faster oscillations appears at  $\sim 59$  MHz. As the external bias further increased, the frequency of oscillations increases slightly and its amplitude decreases monotonously. When the regular oscillations vanishes at 48.5 V, the frequency has shifted to  $\sim 65.1$  MHz. The range of external voltage where the voltage oscillations or instabilities occur is very consistent with the observation of the current plateau. For a heatsink temperature of 9 K, the observed frequencies are lower and the oscillations are not found at all operation points within the plateau.

Concomitant oscillations of the total current (QCL plus voltage probe) measured at the load resistor were also observed and are displayed in Figs. 7(b,d). The current transformer used has a bandwidth of 200 MHz, which limits the resolution here.

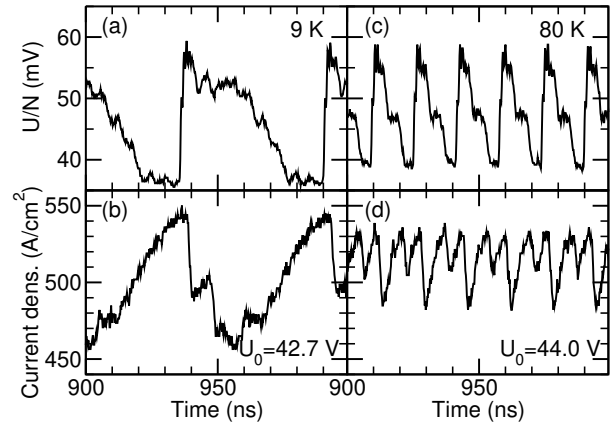


**Fig. 7.** Experimentally detected oscillations at a heat sink temperature of 9 K for a bias  $U_0 = 42.5$  V [panels (a,b)] and at 80 K for  $U_0 = 43.7$  V [panels (c,d)]. The device is operated via a load resistance with  $R = 40.7 \Omega$ . Note that current and bias have been recorded with different cables connecting the cryostat, and that the frequency response of the current and voltage probes are different too, which all together can result to time delays of a few ns between the two signals.

### 5 Simulations with reduced contact conductivity

The experimental observation of oscillations within the second NDC region of Fig. 1 does not agree with the simulated stationary domains discussed in Sec. 3, which are expected due to the stability criterion (8). These stationary field domain distributions show an electron accumulation layer separating the low-field domain close to the injecting contact and the high-field domain at the receiving contact.<sup>1</sup> Such a field distribution is only possible if the contact field  $F_0$  is small at the relevant currents, as otherwise a high-field domain is present at the injecting contact. As discussed in Sec. 3, the stationary domain states require current-densities above  $j_{\min}^{\text{stat}} = 515 \text{ A/cm}^2$  as a consequence of the criterion (7). In the following we use a low contact conductivity  $\sigma/d = 12 \text{ A}/(\text{cm}^2 \text{ mV})$ , where these current densities imply  $F_0 d \geq 43 \text{ mV}$ , which is close to  $F_{\min} d$  at the end of the NDC region. Thus the low-field domain cannot exist at the injecting contact for  $j \gtrsim j_{\min}^{\text{stat}}$  and the stable domain configurations obtained for the second NDC region in Sec. 3 cannot exist. As a consequence we find oscillatory behavior similar to the experimental observation.

Fig. 8 shows oscillatory behavior for a fixed average bias  $U/N = 40$  mV, i.e. in the region of the second plateau. Panel (b) shows a conventional electric field domain distribution at 11 ns. Panel (a) shows that the current density is below  $j_{\min}^{\text{stat}}$  and thus the distribution is not stationary but

<sup>1</sup> Domain distributions with a depletion layer, which have the high-field domain at the injecting contact, are also possible. In order to be stationary, a condition similar to Eq. (8) exists [11], which however requires a substantially higher doping and is not satisfied for our device.

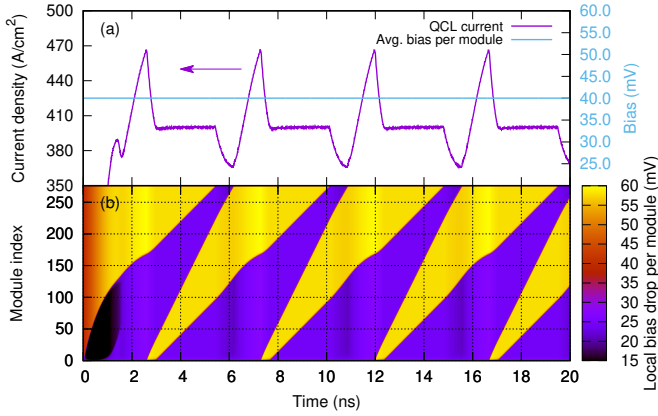


**Fig. 8.** Simulated oscillations in the second plateau for a fixed bias per module of 40 mV applying a reduced contact conductivity  $\sigma/d = 12\text{A}/(\text{cm}^2\text{mV})$ .

travels to the receiving contact. The constant bias provides a raise in the fields and an increase in current. At 12 ns, the field  $F_0$  becomes so large that a high-field domain forms at the injecting contact and starts traveling towards the receiving contact. Simultaneously, the fields drop in all domains and due to the drop of current, the injecting contact can sustain a low-field domain again after 12.5 ns. Afterwards a characteristic period with constant current arises, where the two accumulation fronts travel with half the velocity of the depletion front in between. This scenario is explained in detail for superlattice in Ref. [11]. Around 15 ns one accumulation front and subsequently the depletion front vanish at the receiving contact and the cycle is repeated.

Fig. 9 shows similar domain oscillations under circuit conditions with a load resistor. The frequency is reduced and the signals are altered. Comparing with the electric field distribution in panel (b), we find that the maxima and minima in current from panel (a) are related to the creation of a depletion front at the injection contact and its vanishing at receiving contact, respectively. The corresponding creation and vanishing of the accumulation front is associated with a smaller increase and decrease of slope in the current signal, respectively. The bias behaves precisely the opposite way. Upon varying  $U_0$  we find similar results over the entire second NDC region with average current densities around  $430\text{A}/\text{cm}^2$ . This current plateau (not shown) agrees excellently with the experimental data in Fig. 1 and the simulated oscillation frequencies are comparable (about a factor two larger) to the experiment (at 80 K). However, the particular shapes of the current and bias signal differ, which might be related to more intricate boundary currents  $j_{0 \rightarrow 1}(F_0)$  or to details in the circuit such as a parallel capacitance  $C_p$  not accounted for in our simulations.

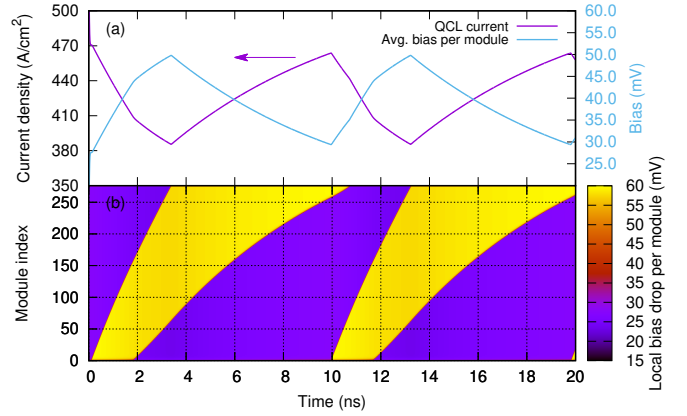


**Fig. 9.** Simulated oscillations in the second plateau for operating via a load resistance of  $50\ \Omega$  and  $U_0 = 41.5\text{V}$  applying a reduced contact conductivity  $\sigma/d = 12\text{A}/(\text{cm}^2\text{mV})$ .

## 6 Conclusion and discussion

We demonstrated both by simulations and experimentally, that oscillating electric field domains are possible in QCLs. Stationary domains are favored by high doping, a large peak to valley ratio  $j_{\text{peak}}/j_{\text{min}}$  in the NDC region and a small excess charge between the domains as quantified by Eq. (8). Furthermore the injecting contact needs to allow for the presence of a low-field domain at its vicinity for current densities above the minimal current  $j_{\text{min}}^{\text{stat}}$  for stationary domain states.  $j_{\text{min}}^{\text{stat}}$  can be estimated by Eq. (7), which, to our knowledge, has not been used before. While the simulated current-bias relations agree well with the experimental data, we did not obtain full agreement regarding the details of the oscillations. In particular, the simulations provide domain oscillations in the first NDC region, which appear to be absent in the experiment. This might be related to a higher background current in the experiment, which counteracts the weak NDC feature. Furthermore, the oscillation signals in the second NDC region differ, which we can not explain now. Finally, we want to point out, that very recently some of us observed domain oscillations in a different QCL, which also persisted after the onset of lasing both experimentally and by simulations [24].

## 7 Acknowledgments

Financial support from the Swedish Science Council (grant 2017-04287) and Nanolund is gratefully acknowledged.

## 8 Authors contributions

Tim Almqvist did the simulations and Emmanuel Dupont the measurements presented here. The numerical codes were developed by Tim Almqvist, David Winge, and Andreas Wacker, who also guided the work. All the authors were involved in the preparation of the manuscript and approved the final version.

## References

1. J. Faist, F. Capasso, D.L. Sivco, C. Sirtori, A.L. Hutchinson, A.Y. Cho, *Science* **264**, 553 (1994)
2. J. Faist, *Quantum Cascade Lasers* (Oxford University Press, Oxford, 2013)
3. M. Razeghi, W. Zhou, S. Slivken, Q.Y. Lu, D. Wu, R. McClintock, *Appl. Opt.* **56**, H30 (2017)
4. B. Röben, X. Lü, M. Hempel, K. Biermann, L. Schrottke, H.T. Grahn, *Opt. Express* **25**, 16282 (2017)
5. F. Capasso, K. Mohammed, A.Y. Cho, *Appl. Phys. Lett.* **48**, 478 (1986)
6. L.L. Chang, L. Esaki, R. Tsu, *Appl. Phys. Lett.* **24**, 593 (1974)
7. J.B. Gunn, *IBM J. Res. Dev.* **8**, 141 (1964)
8. H. Kroemer, *IEEE Trans. Electron Dev.* **ED-13**, 27 (1966)
9. M.P. Shaw, V.V. Mitin, E. Schöll, H.L. Grubin, *The Physics of Instabilities in Solid State Electron Devices* (Plenum Press, New York, 1992)
10. L. Esaki, L.L. Chang, *Phys. Rev. Lett.* **33**, 495 (1974)
11. A. Wacker, *Phys. Rep.* **357**, 1 (2002)
12. L.L. Bonilla, H.T. Grahn, *Rep. Prog. Phys.* **68**, 577 (2005)
13. S.L. Lu, L. Schrottke, S.W. Teitsworth, R. Hey, H.T. Grahn, *Phys. Rev. B* **73**, 033311 (2006)
14. M. Wienold, L. Schrottke, M. Giehler, R. Hey, H.T. Grahn, *J. Appl. Phys.* **109**, 073112 (2011)
15. R.S. Dhar, S.G. Razavipour, E. Dupont, C. Xu, S. Laframboise, Z. Wasilewski, Q. Hu, D. Ban, *Sci. Rep.* **4**, 7183 (2014)
16. C. Sirtori, H. Page, C. Becker, V. Ortiz, *IEEE J. Quantum Elect.* **38**, 547 (2002)
17. E. Dupont, S. Fatholouloumi, Z.R. Wasilewski, G. Aers, S.R. Laframboise, M. Lindskog, S.G. Razavipour, A. Wacker, D. Ban, H.C. Liu, *J. Appl. Phys.* **111**, 073111 (2012)
18. D.O. Winge, M. Franckić, A. Wacker, *Journal of Applied Physics* **120**, 114302 (2016)
19. A. Wacker, E. Schöll, *J. Appl. Phys.* **78**, 7352 (1995)
20. J. Kastrup, H.T. Grahn, K. Ploog, F. Prengel, A. Wacker, E. Schöll, *Appl. Phys. Lett.* **65**, 1808 (1994)
21. L.L. Bonilla, S.W. Teitsworth, *Nonlinear Wave Methods for Charge Transport* (Wiley-VCH, Weinheim, 2010)
22. A. Wacker, M. Moscoso, M. Kindelan, L.L. Bonilla, *Phys. Rev. B* **55**, 2466 (1997)
23. A. Wacker, G. Schwarz, F. Prengel, E. Schöll, J. Kastrup, H.T. Grahn, *Phys. Rev. B* **52**, 13788 (1995)
24. D.O. Winge, E. Dupont, A. Wacker, *Phys. Rev. A* **98**, 023834 (2018)